Water Table Rise in Arid Urban Area Soils Due to Evaporation Impedance and Its Mitigation by Intelligently Designed Capillary Chimney Siphons

Anvar Kacimov[1*], Ali Al-Maktoumi[1,2], Said Al-Ismaily[1], Ahmed Al-Mayahi[1], Afrah Al-Shukaili[1], Yurii Obnosov[3], Osman Abdalla[2,4]

[1]Department of Soils, Water, and Agricultural Engineering, Sultan Qaboos University, Oman.
[2]Water Research Centre, Sultan Qaboos University, Oman,
[3] Institute of Mathematics and Mechanics, Kazan Federal University, Russia ,
[4]Department of Earth Sciences, Sultan Qaboos University, Oman

Emails: anvar@squ.edu.om, akacimov@gmail.com; ORCID: 0000-0003-2543-3219
Email: ali4530@squ.edu.om; ORCID: 0000-0001-8766-5993
Email: esmaily@squ.edu.om; ORCID: 0000-0001-8708-0231
Emails: aalmayahi@squ.edu.om, almayahi.squ@gmail.com; ORCID: 0000-0002-8922-2165
Email: farah93019@gmail.com; ORCID: 0000-0002-7989-4064
Email: yobnosov@kpfu.ru; ORCID ID: 0000-0001-9220-7989
Email: osman@squ.edu.om; ORCID 0000-0001-5150-416X

Short title for running head: Evaporation Impedance and Capillary Siphons

Accepted to Environmental Soil Sciences (Springer)

On August 30, 2021, DOI: 10.1007/s12665-021-09857-3

*Corresponding Author:

Prof. Kacimov A.R.,
Department of Soils, Water and Agricultural Engineering
Sultan Qaboos University Al-Khod 123, PO Box 34 Sultanate of Oman
Tel (968) 24141-201 Fax (968) 24413-418
Emails: anvar@squ.edu.om; akacimov@gmail.com
Omani page:
https://www.squ.edu.om/agr/Academics/Departments/Soil-Water-and-Agricultural-Engineering

Abstract.

Waterlogging of urban area soil in a hyperarid climate, caused by impedance of evapotranspiration due to land cover by an impervious pavement, is studied by a multidisciplinary team of researchers (hydropedeologists, hydrogeologists, groundwater engineers, soil physicists and mathematical modelers). In this paper, a study unique for an arid/hyperarid MENA region has been conducted: from soil pedons' data, a thin vadose zone superjacent to a shallow water table of a coastal aquifer in Oman is described with emphasis on soil profile morphology-layering and determination of the Van Genuchten hydraulic parameters, used in HYDRUS-modeling of evaporation-driven saturated-unsaturated flows. On a large scale, for capillarity-free groundwater flow, the Dupuit-Forchheimer model is used and an analytical solution is obtained. Intensive evaporation from the water table to a bare unpaved soil surface is impeded by an impermeable surface strip (land pavement) with an ensued rise of the water table. Waterlogging is quantified by the "dry area", S_d, under the strip. This integral is explicitly evaluated as a function of the model parameters: aquifer's size and evaporation-normalized conductivity, the width of the strip, d, and its locus with respect to the shoreline, u_1. Nontrivial extremes of $S_d(d,u_1)$ are found.

Contrary to the surface pavement, intensification of evaporation by capillary siphons, i.e. structural heterogeneities of a porous massif, is proposed as an engineering mitigation of groundwater inundation. Composite porous media with siphons (small-size rectangular inclusions of a contrasting finer texture) are numerically tackled by MODFLOW and HYDRUS2D. A constant flux or a constant pressure head condition is imposed on the top of the flow domain. The water table is shown to drop and S_d to increase as a result of such "passive moisture pumping" from the aquifer. A potential model for 2D tension-saturated flow is used to solve a mixed boundary-value problem in a rectangular wick. Its flow rate is analytically evaluated as a function of evaporating width and the height of the "window" through which the aquifer feeds the wick. Conformal mapping of a rectangle in the physical domain onto a rectangle in the complex potential plane is realized via two reference planes and elliptic functions.

Keywords: Capillary siphoning; Aquisalids; Rising water-table; Wetlands; MODFLOW and HYDRUS2D simulations; Vadose zone; Oman.

1. Introduction

In urban groundwater hydrology, cities (entirely or only certain urban areas) are subjected to spatially-temporarily variable hydrological drivers that - in several cases - result in the rise of groundwater levels or "watering up" (see. e.g. Lerner 2003 (pp. 26, 51, 107, 112, 121-122); Vázquez-Suñé et al. 2005; Lerner and Harris 2008; Naik, 2008; Kazemi 2011; Chaudhary 2012; Howard and Israfilov 2012 (pp.6, 32, 35-36, 140-141, 194, 206, 222, 401, 425-426); Jla et al. 2012; Barron et al. 2013; Preene and Fisher 2015; Attard et al. 2016; McCrane 2016; Porse et al. 2016; Vogwill 2016 (pp. 21, 23, 26, 28); Medovar et al. 2018; De Caro et al 2020, Mancini et al., 2020). Schirmer et al. (2013) summarized: *"... over recent decades, in the developed world, abstraction volumes have been reduced and groundwater levels are rising again. Consequently, pumping has to be increasingly*

employed to prevent flooding of underground structures." Minnig et al. (2018) reviewed waterlogging records in Swiss, German and British cities and concluded: "*This increase is mostly due to the reduction in evapotranspiration that more than compensates the increase in runoff produced by the replacement of natural areas (agricultural areas and forests) by impervious surfaces.*"

Urban areas of the Gulf Countries (i.e. Kuwait, Bahrain, Oman, Iraq, Qatar, Saudi Arabia, Egypt and United Arab Emirates) are climatologically similar to arid and hyper-arid cities of California, Iran, Israel, Texas, and Western Australia where a critical rise of shallow water tables (also called "inundation") is caused by:

- leakages from buried fresh water-supply networks,
- return flow from over-irrigation of city parks, municipal and home gardens,
- leakage of untreated sewage water from buried tanks and cesspools,
- lack of storm water and urban drainage aggravated by a historical lack of expertise in dealing with groundwater inundations,
- modification of urban landscapes, in particular, "development" of virgin wadi courses crossing the cities and ensued channeling of runoff into the subsurface at abnormal (to the catchment) infiltration spots,
- infiltration from intensifying natural precipitation,
- stronger groundwater flow through the aquifers located hydraulically upstream of waterlogged city zones i.e. both lateral (unconfined) and ascending (from deep confined formations) groundwater fluxes,

- removal of native vegetation and clearing of deep-rooted perennial plants,

among others (Abu-Rizaiza et al. 1989; Cramer and Hobbs 2002; Saunders 2004; Abu-Rizaiza 2006; Al-Sefry and Şen 2006; Kreibich and Thieken 2008; Al-Senafi 2011;Al-Senafi et al. 2015; Bob et al. 2016; Awad et al., 2020; Essam et al. 2020).

The rise of the water table/piezometric surface in unconfined/confined urban aquifers generates numerous impacts: infrastructural, environmental, social, geotechnical, economic, and ecological. Most of the consequences are undesirable and negative, e.g.:

- differential settlement and cracking of waterlogged buildings,
- cyclic dampening-desiccation and salt crystallization (efflorescence) - dissolution and diffusion of solutes advected by groundwater and vadose zone fluxes into the building foundations with a rapid deterioration of the concrete-masonry strength,
- uplifting and heaving of soil massifs and pavements,
- rutting, structure weakening and damage to the city roads,
- seepage and erosion of buried utility services (pipes, communication cables, tunnels, etc.),
- creation of anoxic condition in the root zone of city vegetation and its perish,
- accumulation of ponded water in depressions (breeding thereof mosquitoes, flies and other insects, and spread of dangerous infections),
- putrefaction in static puddles and pools in basement water with spreading of foul odor,

among others (Abu-Rizaiza 1999; Kreibich et al 2009; Knott et al. 2017; Cardarelli et al., 2016; Aliewi et al. 2020).

Most urban structures in the Gulf countries, however, are not designed to cope with any potential threat/damage of shallow water tables and waterlogging i.e. no drainage have ever been preplanned. Therefore, in most "old" urban districts only hydrological retrofitting and adaptation to rising water tables is feasible.

Even in aquifers subtending European cities, the rise of the water table is not well studied. For instance, Minnig et al. (2018) examined long-term groundwater observation time series for a Swiss city and similar waterlogging trends in England and Germany and concluded that "*Despite an increasing awareness about the need for a better understanding of urban groundwater recharge rates, only few studies on this topic have been performed."* In the arid zone of Arabia, urban groundwater hydrology has only limited data, albeit evaporation from shallow water tables, identified by Minnig et al (2018) as the main hydrological factor in Europe, is an even more important component of the water budget. Therefore, urban development, *viz*. pavement of the land surface and construction of buildings, roads, car parks, etc. drastically reduces evaporation from the phreatic surface, capillary fringe and thin vadose zone, inducing drawup of urban water tables. In this paper, among all the above listed factors causing the rise of shallow urban water tables, we focus only on the impact of urbanization, particularly, pavement of the soil surface. Only one rectification measure, *viz.* amplification of evaporation by siphons is modeled.

In our field and theoretical studies, we selected one subcatchment in Muscat, the capital of Oman, Al-Mawaleh North residential area (coordinates 23° 37' 32'' N, 58° 15' 27'' E, see Image G1 in the Photogallery), located in the coastal zone of the Sea of Oman near the recently renovated Muscat International Airport (formerly Seeb International Airport). The prime location of the area, accelerates its intensive urbanization: construction of residential houses, commercial buildings, extensive interlocking activities (both in the backyards, parking lots, and outside the houses), concrete

pavements and asphalt roads, etc. Additionally and prior to the massive ongoing urbanization activities, the Al-Mawaleh North area used to have many farms and wild vegetation in the past (see the Photogallery, Figure A5). This vegetation have diminished due to salinity or had been abandoned and exterminated due to the expansion of urbanization. The sealing of the ground surface due to pavement and buildings and loss of vegetation has resulted in a lockdown of evaporation and elimination of evaporation and transpiration, respectively. Prior to urban constructions in the 2000-s, the water table was at the depth of 1.8-2.5 m and actively evapotranspired (Kacimov et al., 2009). In recent years, the area is almost permanently inundated, groundwater exfiltrates into nearby topographic depressions that swamps the airport periphery by puddles of stagnant surface water of high salinity. From the critical airport zones, groundwater is now permanently drained by pumping which is costly. The water table depth in the residential area near the airport is very high (0.5-1.5 m, measured from the local ground surface). This situation is common in other coastal areas. For example, in Rome (Italy) the Fiumicino international airport faces a very similar problem, and for that reason the entire area, including the runways, was elevated and brought at a safety level.

Hydrology and hydrogeology of the site as well as the impact of seawater intrusion and tidal effects on the coastal aquifer have been earlier studied (Yechieli and Wood 2002; Kacimov et al. 2009; Kacimov and Abdalla 2010). Groundwater in our case is brackish or saline but we ignore solute transport and density-dependent Darican flows, in particular, convective cells of rotating groundwater in sabkha aquifers. We refer to Figs. 5 and 6 from Wood et al. (2003), where evaporation is sketched as a controlling factor of groundwater motion in a shallow aquifer.

In this paper, we suggest a remedy for potential mitigation of the adverse impact of a risen water table, *viz*. a cheap, “zero-energy” geotechnical solution made of a “capillary siphon” to be constructed on the perimeter of a waterlogged zone, e.g. a building with an affected footing-foundation.

Such siphons can intensify evaporation and create a local, near-building “cone of evaporative depression” or drawdown of the shallow water table. This engineering technique stems from the examination of soil pedology (Subsection 2.1) of the subcatchment, its hydrogeology (Subsection 2.2) and mathematical models (analytical in Section 3 and Appendix and numerical, FDM-MODFLOW in Section 4 and FEM-HYDRUS in Section 5) of saturated and saturated-unsaturated flows of pore water in a shallow aquifer with intensive evaporation. In this paper we are attacking (from different azimuths) the phenomenon of water table rise in an urban area of a hyper-arid country that makes our study unique. However, the phenomenon is also typical not only for one selected site, but rather for the whole Muscat Governorate (Al-Hamami, 2019, Al-Washahi, 2019, Mubarek, 2018), cities in a larger Al-Batinah coastal area in Northern Oman, as well as for coastal cities in UAE, Qatar and Kuwait. The developed analytical solution, MODFLOW and HYDRUS modeling in the paper are, although related to but not limited to the Al-Mawaleh site in Oman. We believe that our results, amalgamate different disciplines related to water flows in natural porous media and converge to understanding shallow water table and vadose zone under evaporation impedance and dewatering by capillary Siphons.

2. Site Description

In this section, we present a field description of the vadose zone with a shallow water table, from the perspective of soil sciences, Subsection 2.1, and hydrogeology, Subsection 2.2.

2.1 Hydropedology of the Site

We explored a coastal zone (see a map in the Photogallery), the North Al-Mawaleh, Oman (elevation about 3 m above mean sea level) by examination and description of soil profiles of excavated pedons, soil sampling, and laboratory analyses (Soil Science Division Staff, 2017). The soils of the study area are of an alluvium origin, occurring on a flood plain, and are formed from the deposition of wadis originated from the nearby Al-Hajar Mountains. The texture of these soils is generally silty (fine loamy or fine silty). The site is dominated by Aquisalids (salt-enriched Aridisols experiencing wet soil moisture conditions, see the taxonomy in Soil Survey Staff, 1992), or locally known as Sabkha (salt scald). The genesis of the Aquisalids is governed by the existence of three conditions (Boettinger and Richardson 2001), viz. there must be

(i) a shallow or rising water level;

(ii) a source of ions or dissolved minerals that are transported by water; and

(iii) a process of solutes concentration and ultimately crystallization(i.e. in the hydrologic cycle evapotranspiration exceeds infiltration and leaching of solutes)

The Mawaleh Aquisalids are periodically saturated in the sub-horizons within 100 cm and for more than one month per year. These soils are subjected to a fluctuating saline water table monitored there in boreholes, pedons excavations and geophysically (see Fig. P1 of the attached Photogallery, the Electronic Supplementary File). The detected saline shallow water table is mainly due to the seawater intrusion of Al-Batinah coastal plain (Kacimov et al., 2009).

Some patches of the Aqusalids soils of this area form gleying and redoximorphic features in the sub-layers that are normally frequently saturated with the shallow water (Fig. P2a,b). The Aqusalids in our case are of fine silty texture, silt exceeds 40%, and may reach more than 90% in the sub-layers (see Table 1). They are rich with calcium carbonates (we detected moderate to strong effervescence with addition of 1*M* HCl), with an average pH of 7.0. These soils are morphologically characterized by having a very saline salt accumulation in the forms of quasi round shiny salt crystals, with a distinct white, thin, and brittle surface salt crust (Fig. P3). There is a pedogenic salic subsurface diagnostic horizon (Fig. P4). Raised salty-polygonal patterns topped with rounded granularly-shaped salt crystals in some places (Fig. P5a,b) are evident. Soft, often moist, friable, puffy feeling, surface and lumpy microrelief (about 2.5 cm height) and surface heaving of few centimeters are among the morphological features formed in these soils (Fig. P6). This lumpy or bubble-like, blistered appearance may result from a combination of surface inundation and subsurface evaporation (Lines, 1979).

We recall that in Aquisalids that are flooded periodically, individual salt crystals reported to have rounded (Fig. P5b) rather than sharp edges (Lichvar et al., 2006). The EC_e values of the Aqusalids soil layers, which we measured, ranged from 30 to 150 dS/m and with more tendency for the salts to accumulate in the top layers (Table 1). High evapotranspiration rates with a pronounced dry season, availability of salt-laden and subsequent capillary input from groundwater, and frequent flood events create conducive and invasive conditions for the development of top and subsurface salt-associated morphological features in the soil pedons of North Al-Mawaleh area. The depth of the salic horizon (Fig. P4) varies seasonally depending on the amount, seasonality, and intensity of precipitation, fluctuation, and shallowness of the saline water table, and the rate of capillarity-evaporation induced vertical moisture flows. The presence of the brittle salt crust (Fig. P3), formed due to evaporation from the capillary fringe, in the top of these

soils is an indication of periodic saturation in the upper part of these soils from a rising saline water table. Aquisalids that are experiencing water ponding during part of the year usually develop brittle salt crust morphology on the soil surface (Boettinger 1997).

We found cryptobiotic crusts (also known as biological soil crusts, cryptogamic crusts, or desert algal crusts) on the top of few soil spots of the North Al-Mawaleh Aqusalids close to Muscat International Airport (Fig. P7). These biocrusts appear like a smooth carpet, dark beige in color and with a distinct green cast on their underside, and either intact or peeled off. Darker biocrusts are usually dominated by algae and provide evidence of ponding with several wet-dry cycles, which is the case in our study area (Brostoff et al., 2002).

Table 1: Soil profile description of the Aquisalids of North Al-Mawaleh area.

Horizon	Depth (cm)	Structure	Boundary	Munsell Colour (Moist)	Sand %	Silt %	Clay %	Sand Fractions (%)						Textural Class	Effer -vescence	ECe (dS/m)	pHe
								1 mm	500 µm	250 µm	106 µm	53 µm	<53 µm				
Az (Thin salt crust)	0-19	Granular	Very abrupt smooth	10YR 4/4	25.5	62.0	12.5	43.0	24.7	13.9	10.0	4.2	3.0	Silt Loam	Strong	147.2	6.5
Akz	19-31	Granular	Very abrupt smooth	10YR 4/6	46.5	43.4	10.1	35.1	26.8	17.7	11.9	7.1	0.9	Clay Loam	Strong	91.5	7.0
Bz	31-49	Granular	Clear	10YR 5/4	17.4	79.0	3.6	38.2	28.6	11.7	12.1	4.4	4.5	Silt Loam	Moderate	73.0	7.2

			smooth													
Cz	49-67	Massive	Gradual smooth	10YR 6/4	13.2	84.3	2.6	34.2	36.2	17.9	6.9	2.0	1.5	Silt	Moderate	43.3	7.3
Cg	67-115	Massive	Gradual smooth	10YR 6/3	7.3	91.7	1.0	49.3	26.3	8.8	8.4	2.8	3.5	Silt	Moderate	32.1	7.4

2.2 Hydrogeology and Geology

The site under investigation is a low-lying coastal plain. A thick pile of sediments is deposited in the area during Tertiary and Quaternary time and two major distinctive stratigraphic units were formed: Fars Group and Quaternary Alluvium. Fars Group, which is a shallow marine-sabkha combination of dominantly carbonate rocks with gypsum and halite, is encountered at a greater depth beyond the interest of the current study. The alluvium, which is located at the top of the stratigraphic succession, comprises an unconsolidated mixture of poorly sorted gravels, sands, silts, and clays with variable grain size and shape. The alluvium accommodates a significant load of carbonate and evaporite cement due to water circulation and evaporation. The site proximity to sea encourages seawater flow over the plain surface during high tides through creeks locally known as “Khors”. Subsequently, ponds of seawater form on the ground surface and undergo evaporation that enhances salt accumulation and infiltration that carries salts down to the subsurface.

A regional unconfined groundwater flow system occurs from relatively elevated mountains located a few kilometers to further south (characterized by a relatively steep hydraulic gradient). Fresh groundwater in the upper unconfined aquifer made of recent alluvium “collides” with denser saline groundwater, which moves from the shoreline (a vertical segment E_3M_3) in Fig.1a inland. The intruded seawater mixes with the natural groundwater system and forms a transitional diffusive zone (in terms of salinity content) that is characterized by a density contrast between the two zones (fresh and saline water) and therefore constitutes a hydrological no-flow boundary, often modeled as a sharp interface (Strack, 1989). In Fig.1a, such an interface is located far to the left with respect to the leftmost boundary, *OFC*, of the flow domain. Therefore, all subsurface water in the flow domain in Fig.1a is saline. The sharp interface (not shown in Fig.1a) acts as a piston, which, unlike “common” seawater intrusion scenarios (Strack, 1989), thwarts any hydraulic contact between fresh groundwater and the open body of the sea. This interface is a mathematical separatrix with two stagnation points. Such flow topology is

193 described by Kacimov et al. (2009) and is practically evidenced by the phreatic surface dipping
194 from point M_3 inland. Water tables located below the mean sea level are also detected in a
195 coastal aquifer near Rome, Italy (see Capelli et al., 2007, Mancini et al., 2020).

196 The inland hydraulic gradients along the whole segment E_3M_3 in Fig.1a for a steady state
197 seepage (studied below in Section 3) are possible if a "sink" of saline groundwater exists. In
198 arid-hyperarid climatic conditions of Oman evaporation from a shallow water table acts as such a
199 "distributed sink" illustrated by vertical arrows in Fig.1a.

200 **3. Analytical Solution: Dupuit-Forchheimer's Flow in Unconfined Aquifer With**
201 **Partially Occluded Evaporation**

202 In this section, we present an analytical solution to the problem of groundwater flow on a
203 subcatchment scale. No wick-wall is installed.

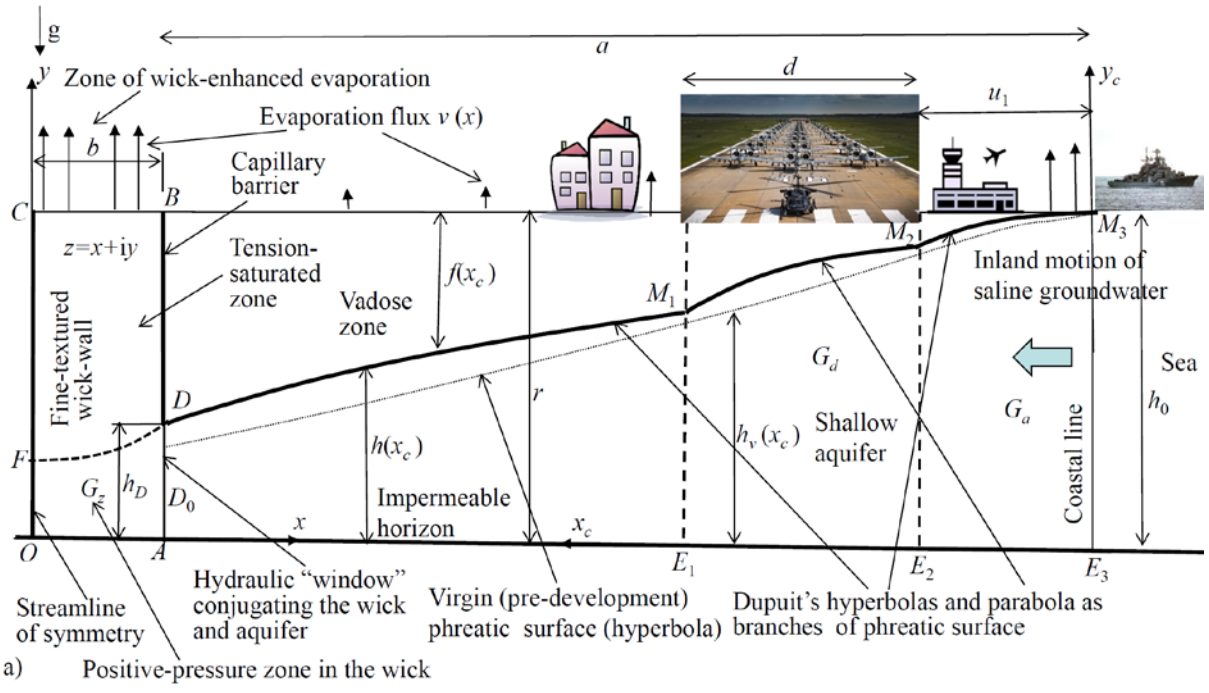

204

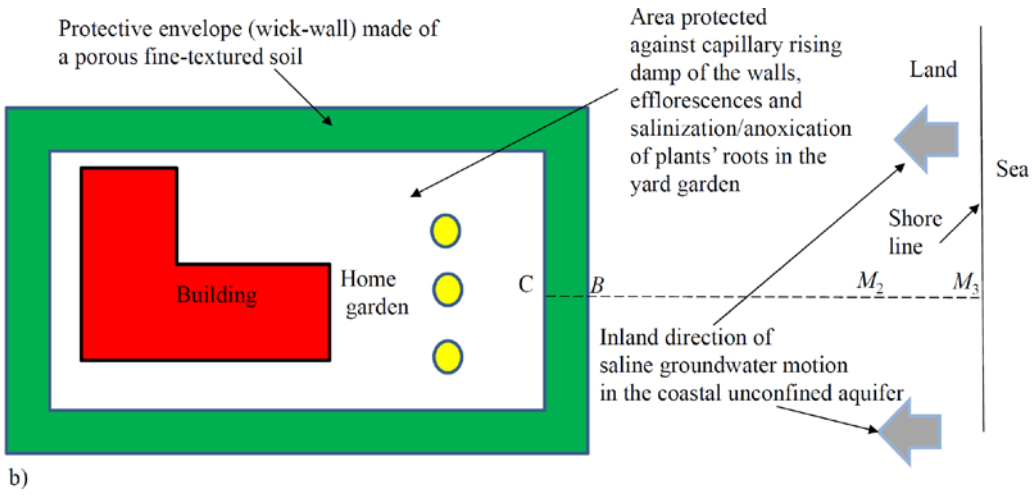

205

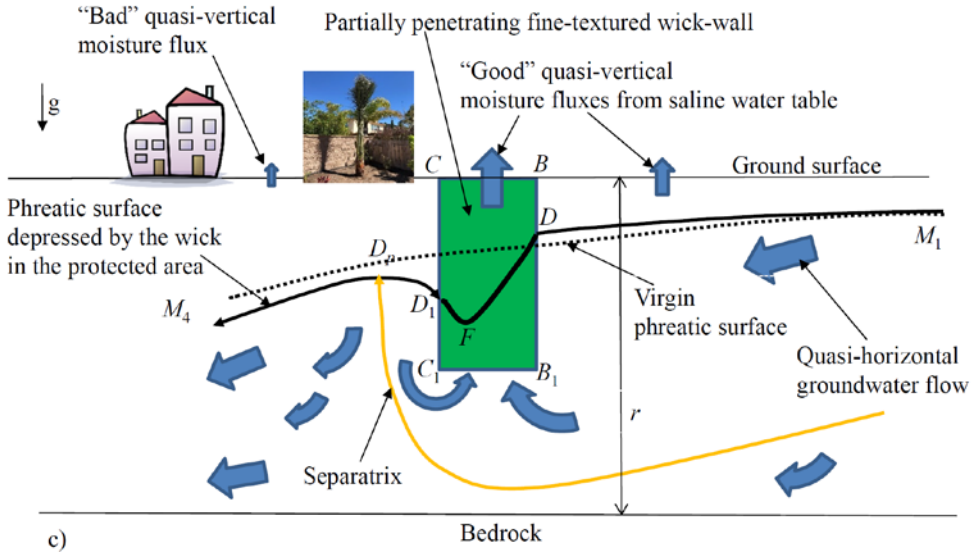

206

207 **Fig. 1.** a) Vertical cross-section of an unconfined coastal aquifer. Seawater seeps through a
208 vertical coastal segment E_3M_3 and moves over an impermeable horizon inland, driven by
209 evaporation from the ground surface CBM_3. The left-most boundary, a vertical segment *ADB*,
210 An strip impervious to evaporation of the land surface has a width *d* and located distance u_1
211 from the shoreline. A fully-penetrating wick-wall *OCBA* of a width *b* is made of fine-textured
212 soil (impeding and facilitating evaporation). The wick-wall may be located on the left of a
213 vertical segment *ADB*, distance *a* from the shoreline. If no wick, then *ADB* is impermeable; b)
214 aerial view of a rectangular area protected by a wick-wall; c) groundwater flow topology in the
215 vicinity of a partially-penetrating wick-wall (vertical cross-section).

216 Fig.1a depicts a vertical cross-section of an unconfined aquifer based on a horizontal bedrock
217 OAE_3. The thickness of the porous material, *r*, is constant (topography of the study area is flat,
218 see Subsection 2.1). The saturated hydraulic conductivity K_s and the Van Genuchten (VG) soil
219 hydraulic parameters ($\alpha, n, \theta_r, \theta_s$) are assumed to be constant (Simunek et al. 2016). We introduce
220 two systems of Cartesian coordinates: O*xy*, and $E_3x_cy_c$ (Fig.1a). The shoreline E_3M_3 is vertical.

The seawater level is h_0 and density, ρ, of groundwater, are constants. We define the piezometric head in the unconfined aquifer as $h = p + y_c$ where p is the pressure head such that along the segment $x = 0$ the head is $h = h_0$.

In this section, we assume that the line ADB ($x_c = a$) is a vertical no-flow boundary. Kacimov et al. (2009) showed that on the catchment scale in the Al-Batinah region of Oman (x~ 20-50 km), ADB in Fig.1 can be considered as an interface between saline and fresh groundwater, albeit the real interface is not vertical.

In our study area, the distances $a = |AE_3|$ is about 1 km, u_1 ~ tens to hundreds of meters, and d ~ meters to tens of meters. These are approximate sizes of the Muscat International Airport in the direction of the E_3x axis and a coastal urban district nearby (correspondingly). In our analytical solution below, the sizes a, u_1 and d are arbitrary, provided the Dupuit-Forchheimer (DF) approximation is valid i.e. h_0/a is small.

Prior to the land development, a virgin water table was M_3D_0 (Fig.1, dotted line) and its saturated thickness was h_v (x_c). M_3D_0 dipped inland due to natural (direct) evaporation and transpiration from a horizontal soil surface M_3B. The curve D_0M_3 is hyperbola (PK-62) for unimpeded evaporation of a constant intensity.

The evaporation rate, e, generally, depends on the VG soil properties and atmospheric conditions, decreasing with the depth $f(x_c)$ as depicted by vertical arrows of varying length in Fig.1 (Polubarinova-Kochina 1977, hereafter abbreviated as PK-77, Kacimov et al. 2019a, 2021a). In this section, we follow the simplest PK-77 model which assumes that e is constant.

The land cover (pavement, construction of buildings, roads, airport's runway, etc.), in Fig. 1a is modeled by a strip of width d. Under this strip $e = 0$ (no evaporation from the water table). Due to the land cover in urban development, the water table $M_3M_2M_1D$ has risen as compared with the virgin level. Physically, the curve $M_3M_2M_1D$ monotonically decreases

landward and is smooth but in Fig.1a the water table is depicted with “corners” at points M_1 and M_2.

We aim to determine the saturated thickness $h_c(x)$ under $M_3M_2M_1D$ as a function of d and u_1. Of special interest is the branch M_1M_2, which determines waterlogging under the airport runway (or building foundation). In particular, we are interested, whether - at a given d - the locus of the construction ($a - d < u_1 < 0$) can be selected within the subcatchment of Fig.1 in such a manner that waterlogging under a zone of utmost importance can be made minimal.

In the DF model (Strack 1989), steady 1-D flow in the aquifer of Fig.1obeys the ODE:

$$\frac{\mathrm{d}^2F_s(x_c)}{\mathrm{d}x_c^{\,2}} = \begin{cases} e/K_s, & 0 \le x_c \le u_1,\ \ u_1 + d \le x_c \le a, \\ 0, & u_1 < x_c \le u_1 + d, \end{cases}$$
$$F_s(x_c) = \frac{h^2}{2}, \quad q = -K_s h \frac{\mathrm{d}h}{\mathrm{d}x_c} = -K_s \frac{\mathrm{d}F_s}{\mathrm{d}x_c}, \tag{1}$$

where F_s is the Strack (1989) potential and q is the comprehensive discharge (total seepage flow rate in each cross-section of the aquifer). Usually (see e.g. Coffey and Shaw, Cohen and Rothman 2017; Haitjema 1995, PK-77; Strack, 1989), e in the RHS in eqn. (1) is negative (accretion to the water table). A 2-D potential model for a phreatic flow with evaporation was used by Craster (1994).

The boundary conditions for ODE (1) are:

$$F_s(0) = \frac{h_0^2}{2}, \quad \frac{\mathrm{d}F_s(a)}{\mathrm{d}x_c} = 0\,. \tag{2}$$

The first equation (2) means that the seawater level at x_c=0 (a vertical segment M_3E_3 in Fig.1a) is h_0 i.e. constant. Tide effects, studied earlier in the same area both analytically and experimentally by Kacimov and Abdalla (2010), are neglected. The second equation (2) assumes a no-flow boundary at x_c=a (segment AB). If no protection by a wick-wall by pavement above a horizontal segment E_1E_2, then the analytical solution is extended to the sharp interface as in Kacimov et al. (2009), i.e. a is several kilometers. Consequently, AB models a real, almost

vertical interface-streamline. If the scale is smaller, a is several hundred meters and we deal with a wick-wall as the left boundary of the Dupuit-Forchheimer flow, then the flow domain is bounded from the left by a perfect, fully penetrating low-permeable wall, *ABCO*, as in Fig.1a, or a partially penetrating wall, BCC_1B_1, in Fig.1c. In case of both types of walls, the no-flow condition in eqn. (2) is not exact. Obviously, F_s and its first derivative are continuous at $x_c = u_1$ and $x_c = u_1 + d$.

The solution to BVP (1)-(2) is explicitly obtained[1] and gives two hyperbolas M_2M_3 and M_1D and a Dupuit parabola M_2M_1.

We introduce dimensionless quantities: $(x_c^*, u_1^*, d^*, h_0^*) = (x_c, u_1, d, h_0)/a$, $S_d^* = S_d/a^2$, $q^* = q/(K_{s1}a)$, $e^* = e/K_{s1}$ and drop for them the superscript "*".

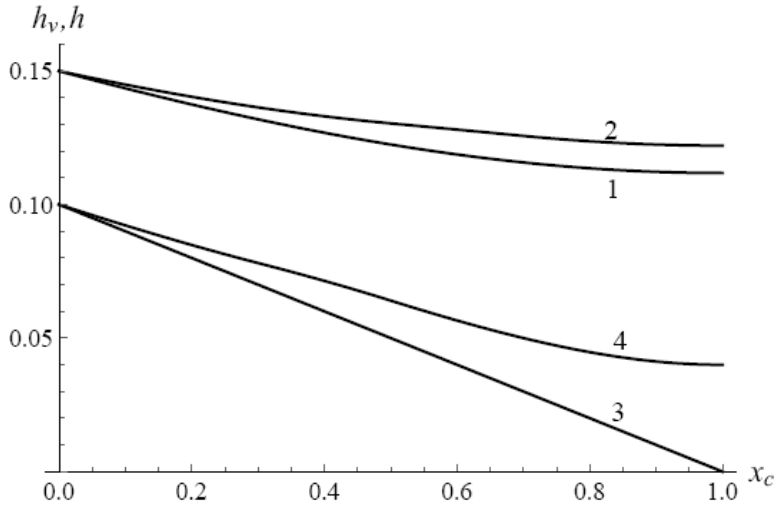

Fig. 2. Virgin and evaporation-eliminated water tables $h(x_c)$ and $h_v(x_c)$ for $h_0 = 0.15$, $e = 0.01$, $u_1 = 0.5$, $d = 0.2$ (curves 1 and 2, respectively). Curves 3 and 4 are plotted for $h_0 = 0.1$, $e = 0.01$, $u_1 = 0.3$, $d = 0.2$.

Fig.2 shows $h(x_c)$ and $h_v(x_c)$ for the tetrad of dimensionless parameters (h_0, e, u_1, d) = (0.15,0.01,0.5,0.2) (curves 1 and 2, respectively). Curves 3 and 4 (virgin and pavement-hoisted water tables) are plotted for the tetrad (0.1, 0.01,0.3,0.2).

We define a "dry area" above the branch M_1M_2 of the phreatic surface and beneath the evaporation-impeded strip in Fig.1 as

[1]We skip it here for the sake of brevity

$$S_d = d\,h_0 - \int_{u_1}^{u_1+d} h(x_c)\mathrm{d}x_c \cdot \tag{3}$$

This area of a curvilinear trapezium G_d (Fig.1) can be considered as an integral criterion of waterlogging of the *d*-strip.

The integral in eqn. (3) is explicitly evaluated:

$$S_d(h_0, e, u_1, d) = d\,h_0 + \frac{\left(h_0^{\,2} + e\,u_1\left(u_1 - 2 + 2d\right)\right)^{3/2} - \left(h_0^{\,2} + e\,u_1\left(u_1 - 2\right) + 2ed\ \left(2u_1 - 1 + d\right)\right)^{3/2}}{3e\left(u_1 - 1 + d\right)}. \tag{4}$$

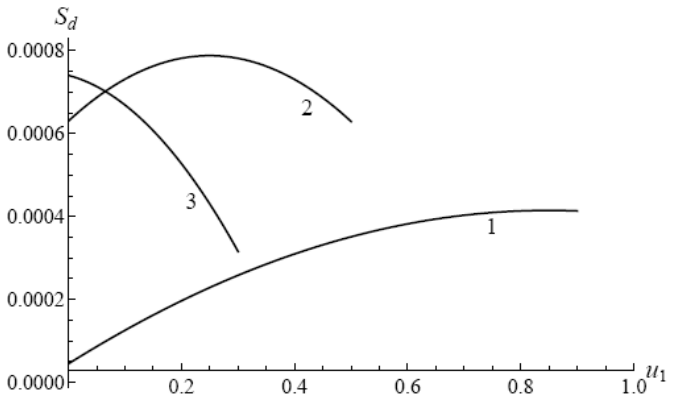

Fig.3 "Dry area" S_d as a function of u_1 for three strip width d = 0.1, 0.5 and 0.7 (curves 1-3) at h_0 = 0.1 and e = 0.001.

In Fig.3, we plot $S_d(u_1)$, expressed by eqn.(4), for d = 0.1, 0.5 and 0.7 (curves 1-3) at h_0 = 0.1 and e = 0.001. Extrema are found from eqn.(4) using the **FindMaximum** routine of *Mathematica* (Wolfram, 1991). For example, curves 1 and 2 have the maxima ($S_{dM,}$ u_{1M}) = (0.000415, 0.85) and (0.00079, 0.25), correspondingly, while curve 3 illustrates only a monotonically decreasing $S_d(u_1)$ and only an end maximum.

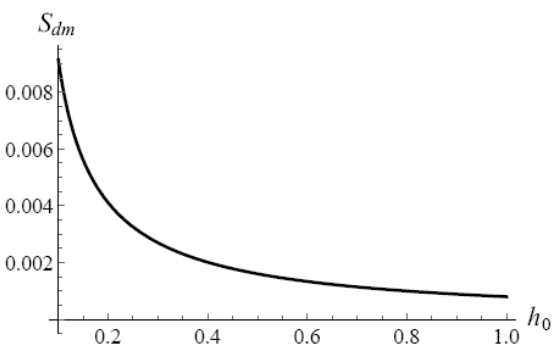

a)

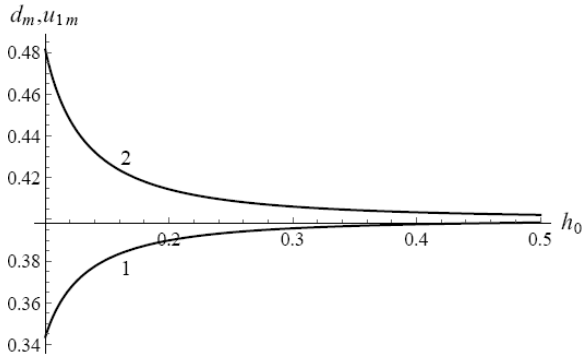

b)

Fig.4. a) Maximal (optimal) "dry area" S_{dm} as a function of h_0 for $e_0 = 0.01$.

b) Optimal $u_{1m}(h_0)$ and $d_m(h_0)$ (curves 1, 2, correspondingly) for $e_0 = 0.01$.

Let us consider both u_1 and d as design (control) variables. That means the land developers can:

a) locate a pavement in the catchment as they wish,

b) can vary its width.

The **FindMaximum** routine applied to $S_d(u_1,d)$ determines the best (in the sense of the "dry area" criterion of eqn.3) scenario i.e. the optimal triad (S_{dm}, u_{1m}, d_m), provided, that the dyad (h_0, e) is fixed. The found optima can be further analyzed. For example, Fig. 4a and Fig. 4b plot $S_{dm}(h_0)$ and $u_{1m}(h_0)$, $d_m(h_0)$ (curves 1, 2, correspondingly) for $e_0 = 0.01$. These graphs can be also used for isoperimetric estimates and sensitivity analysis (Ilyinsky and Kacimov, 1991) of waterlogging. Fig.4 illustrates that for a broad variation of h_0 the optimal values (u_{1m}, d_m) do not vary much while the objective function S_{dm} does.

The concept of a wick-wall is illustrated in Fig.1b,c. An area (a white rectangle in Fig.1b) to be protected against waterlogging can be a building with a home garden. A trench of a width b is dug as a "green" envelope surrounding the protected area. The trench is filled with a material finer than the ambient (background) soil. The trench can fully penetrate the vadose zone and unconfined aquifer (if they are thin enough) as in Fig.1a or only partially as in Fig.1c. The trench filling acts as a wick for groundwater and soil moisture. As result of a continuous wicking, the interior of the protected area in Fig.1b is dewatered. A smart heterogenization of soil aimed at reducing evaporation from a shallow water table has been recently examined by Al-Shukaily et al. (2019), Kacimov et al. (2019b).

4. MODFLOW Simulation: Groundwater Flow in Aquifer With Evaporation Impeded by Surface Pavement and Intensified by a Peripheral Capillary Siphon

In this section, a shallow unconfined aquifer (analytically modeled in Section 3 at the scale of Fig.1a) is simulated using a Finite Difference Method (FDM) implemented in the code MODFLOW 2005 (Simcore, 2012). The wick-wall fully penetrates the aquifer.

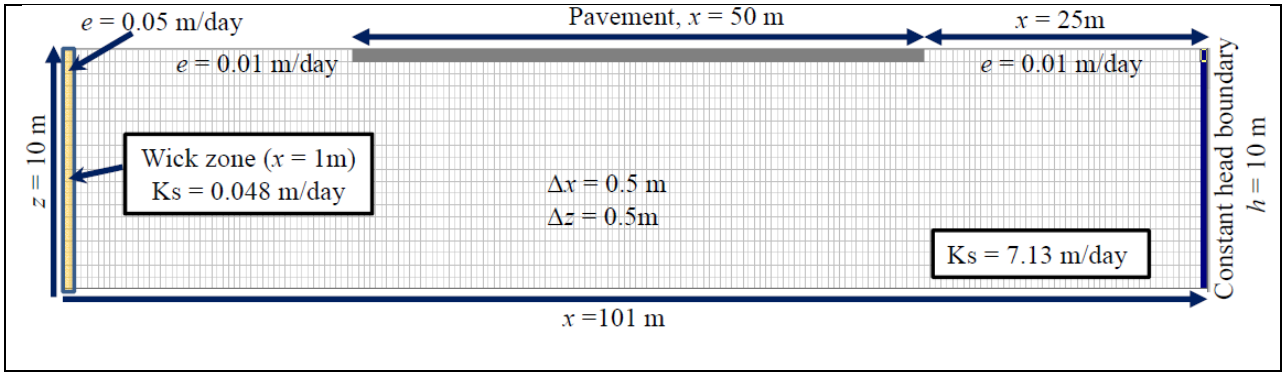

Fig. 5. A vertical cross-section of a rectangular flow domain for the problem simulated by MODFLOW.

Fig. 5 depicts a vertical cross-section of the MODFLOW domain subtended by an impermeable horizontal bedrock. This flow domain corresponds to the transect M_3M_2BC in Fig.1b.

The MODFLOW simulations were specifically designed to intertwine with the analytical approach and HYDRUS runs (Section 5) with an overarching goal of illustrating the commonality of all the three models. Correspondingly, the following assumptions were made: steady-state flow conditions, bedrock is at depth of 10 m, and high effective porosity. The hydraulic conductivity K_s for the main aquifer and wicking zone on the left is 7.13 m/day and 0.048 m/day, respectively. These K_s values are selected from the HYDRUS Soil Catalogue for sand and clay (see Section 5 below where sand and loam were selected as hydraulically contrasting components of composites). The effective porosity is 0.4 for the wicking zone and 0.2 for the aquifer. The domain is gridded with 20 rows and 202 columns, forming a total number of 4,040 active cells, with the cell sizes of $\Delta y = \Delta x = 0.5$ m. The Generalized Conjugate Gradient method with preconditioning, involving a “Modified Incomplete Cholesky” solver, was

selected with a convergence criterion of 0.001. The constant head at the right boundary is $h_1 = 0$ m (Fig. 5); the left-most boundary of the rectangle in Fig.5 is impermeable (as in Section 3). The no-flow pavement segment is 50 m wide and its right rim is located 25 m from the inflow boundary, as shown in Fig. 5. An evaporation rate of 0.01 m/day is assigned for the unpaved top of the aquifer and 0.05 m/day at the top of the wicking zone (a fine-textured wick is wetter due to its higher capillarity and evaporates more). Similar to Section 3, MODFLOW models the saturated zone only with a "sink term", *e*, in Fig.5 quantifying the hydrological effect of the vadose zone. Two scenarios were run: with a yellow strip in Fig.6 (wick) and without this wick.

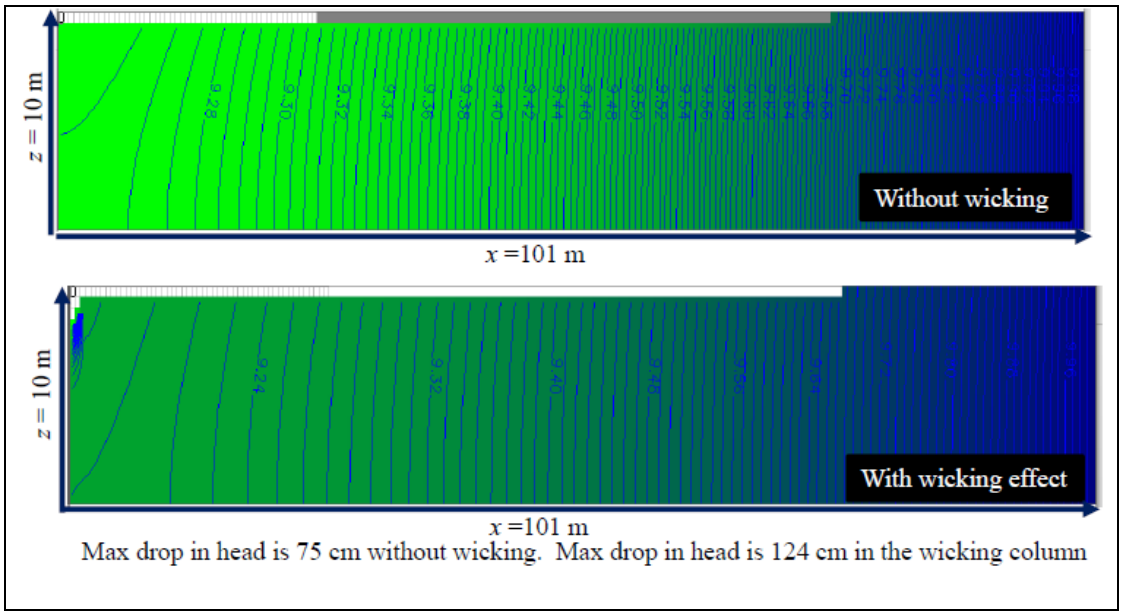

Fig.6. MODFLOW-computed equipotential lines without capillary with and without wick (upper and lower panels).

Fig.6 presents the equipotential lines for the two cases, with an illustration of a stronger drawdown with a wicking strip.

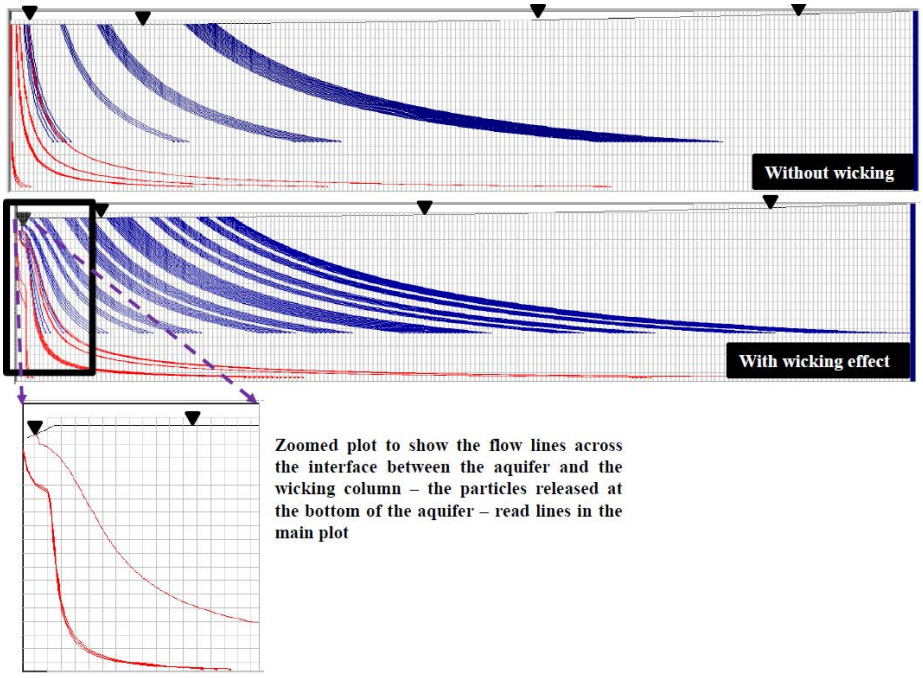

359

360 **Fig.7.** MODFLOW streamlines for flow without a wick (upper panel), with wick (middle
361 panel) and refraction in a zoomed zone close to the interface between two subdomains of
362 contrasting conductivity (lower panel).

363 Fig.7, the upper panel represents the paths of marked particles released at different locales
364 within the flow domains without a wick. The middle panel represents the streamlines for flow
365 bounded by a right-wing wick. The lower panel zooms the vicinity of the vertical interface
366 between the aquifer and wick where streamlines experience a strong refraction.

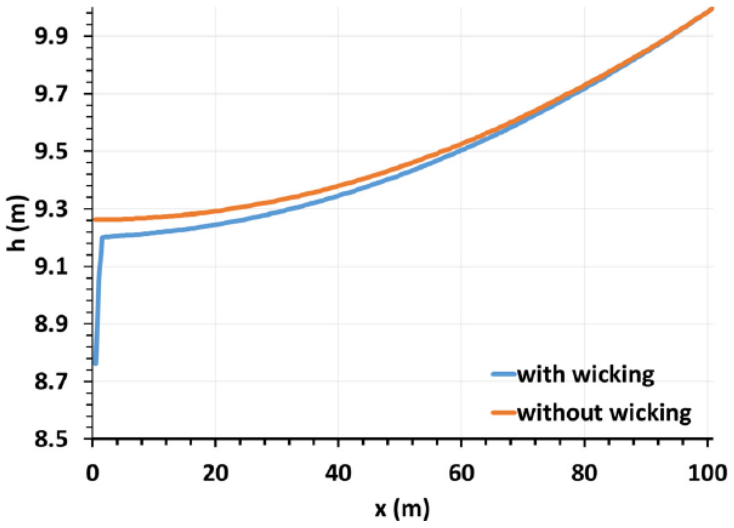

367

368 **Fig.8.** Water tables for homogeneous and composite aquifers.

The water tables are shown in Fig.8 for the two scenarios. A relatively thin wick significantly reduced groundwater flooding under the paved area in Fig.5.

5. HYDRUS Simulations of Saturated-Unsaturated Flow With Structurally Obstructed-Augmented Evaporation

In this Section, we modeled porous composites that optimize drainage of soil water under an impermeable surface structure without and with an evaporating wick-wall. Like in Sections 3-4 above we first evaluate what is the waterlogging effect of the blockade of evaporation from a shallow water table. After that, we compute the dewatering action of a fine-textured porous siphon.

Similar moisture siphoning techniques sucking water from a shallow phreatic surface have been recently implemented at the scale of pots, barrels, raised beds, and small cultivated crop fields in agronomy and cultivation of ornamental plants in arid regions (Al-Mayahi et al. 2020; Al-Mazroui et al. 2020).

Below, we examined 1-,2-D saturated-unsaturated Darcian flows from a horizontal water table to a dry soil surface using HYDRUS2D (Šimůnek et al. 2016), which solves Richards' equation. Unlike models of a relatively large horizontal scale (hundreds of meters-kilometers) in Sections 3 and 4, here we considered smaller flow domains stretched for meters and tens of meters. Correspondingly, we operated with a vadose zone above a shallow water table (see Subsection 2.1 and Photogallery, Figs. P1-P5).

In Subsection 5.1 we considered a model of evaporation in a pristine coastal sabkha, prior to urbanization (see Subsection 2.1), with no pavement or any other urban disturbance of the ground surface. In this case, evaporation through a five-strata vadose zone is 1-D. In Subsection 5.2, we modeled three different scenarios:

1) 1-D evaporation through a homogeneous sandy soil having “effective” properties, with no building (pavement) on the ground surface.
2) 2-D flow to the soil surface which, similarly to Sections 3-4, has an impermeable segment (footing of a building) but no wick-wall. The strip of homogeneous soil in a vertical cross-section experiences a considerable waterlogging due to impeded evaporation.
3) 2-D flow in the same rectangle as in scenario 2, but with two rectangular fully-penetrating wick-walls made of loam, added on the left and right rims of the foundation for amplification of evaporation by wicking through these artificial buried walls. A certain desaturation of the soil under the protected foundation of the building is attained.

5.1 1-D *evaporation from a shallow water table through a five-layered vadose zone*

Evaporation through the five-layered soil profile was simulated by HYDRUS2D for 10 years (3,650 days) using default options for initial time steps and the maximum number of iterations. Constant pressure heads p = -1000 cm and p = 0 were applied at the topsoil and water table. We recall that a default HYDRUS notation for the pressure head is h (not to be confused with the piezometric head in the previous Sections). The percentage of sand, silt, and clay for each layer were retrieved from Table 1 (Section 2.1) and inserted as inputs into the Neural Network Prediction of HYDRUS to get the hexad of VG parameters for each layer (Table 2). After that, the effective harmonic and geometric mean values of K_s for a homogenized layer (see Yeh et al., 2015) and VG parameters for all layers were calculated (Table 2). We used the default HYDRUS VG parameters for sand and loam in simulations of Subsection 5.2. We recall that in saturated flows across layers (in our case, 1-D evaporation through a layered soil) the effective hydraulic conductivity is evaluated as a harmonic mean, meanwhile a geometric mean is a better effective value in 2-D flows (Kacimov and Obnosov, 1997, Yeh et al., 2015, p.240). The isobars at the final time of simulations i.e. t =10 for the five-layered soil profile are shown in Fig. 9.

Table 2: Hexad of VG soil properties for five layers of the soil profile in Table 1: θ_r and θ_s are the residual and saturated volumetric water contents, respectively; α and n are shape parameters of the water retention curve; and K_s and L_C denote the saturated hydraulic conductivity and pore connectivity parameter, respectively.

Horizon	θ_r	θ_s	α	n	K_s(cm/day)	L_C
Az	0.055	0.426	0.004	1.696	28.880	0.5
Akz	0.043	0.396	0.010	1.509	25.230	0.5
Bz	0.043	0.492	0.006	1.705	66.130	0.5
Cz	0.043	0.515	0.007	1.683	66.050	0.5
Cg	0.043	0.550	0.010	1.650	63.570	0.5
Effective parameter (harmonic mean)	0.044	0.492	0.007	1.655	47.261	0.5
Effective parameter (geometric mean)	0.045	0.472	0.007	1.647	45.836	0.5

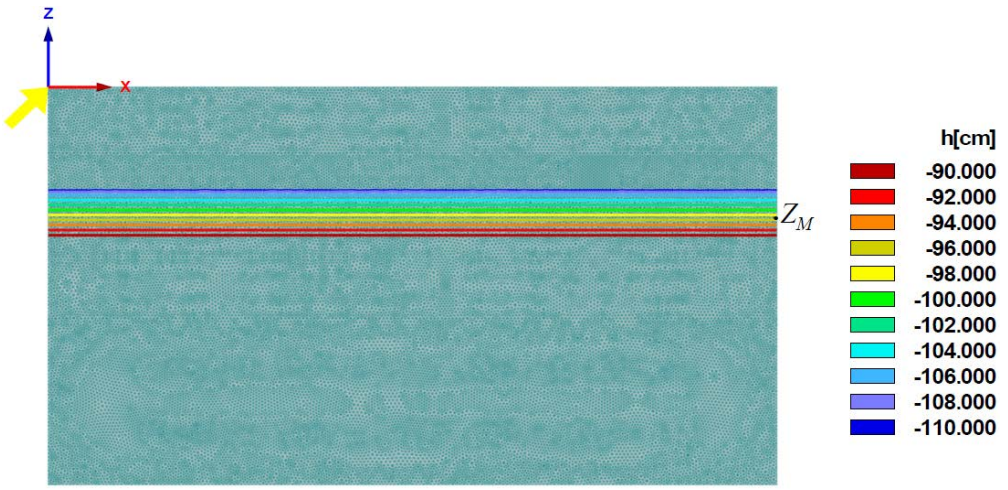

Fig.9. HYDRUS isobars at t = 3650 days for a pristine five-layered soil profile from the Al-Mawaleh site.

5.2 2-D *unsaturated flow from shallow water table under a building foundation*

In this Subsection, we considered 2D unsaturated flow in an area with a shallow water table. Due to symmetry, we modeled a right half of the flow domain: a rectangle x = 200 cm, z = 100 cm (Fig. 10). For scenario 1, the domain was made of a homogeneous sandy soil selected from the default HYDRUS catalog. The domain was initially at the pressure head p = -100 cm and we assumed the upper and lower boundaries to be subject to conditions p = -1000 cm and p

= 0 cm, respectively. No flow boundary was set to both left and right boundaries of the rectangles.

For the second scenario, we used the same domain and boundary conditions of the first scenario, except that a 100 cm-long topsoil segment 100 cm < x < 200 cm (building's foundation) was a no-flow boundary. The initial conditions of this scenario were imported from the final time layer of scenario 1.

In the third scenario, a rectangular fully penetrating wick made of loam was inserted at the left boundary of the flow domain (similarly to the MODFLOW wicking model in Section 4). The wick was 50 cm wide and 100 cm deep. All boundary conditions for this scenario were the same as in scenario 2. The initial condition was imported from the final time layer of the second scenario.

We did a grid and time resolutions analysis to ensure the accuracy and stability of modeling. The grid was varied from a coarse mesh size of 5.6 cm to a fine mesh of 1 cm. The impact of time on simulation results was evaluated to ensure a targeted steady-state flow. Ten years of simulation time (3650 days) were found to suffice for evaporation-driven steady groundwater and moisture motion in each scenario.

We quantified waterlogging of the foundation zone by the isobar $z_{100}(x)$ which corresponds to p = -100 cm (pale green lines in Fig.11). Any other HYDRUS isobar double-bounded by the inequality $0 < |p| < 1000$ can be selected. Two criteria of waterlogging were used:

- the locus, $z_M = z_{100}(200)$, of the apex of the isobar (Figs. 9 and 11),

and

- the area, S_{100}, of the rectangle above this selected contour line.

The area as an integral criterion of waterlogging was evaluated in the following manner: we imported from HYDRUS to *Mathematica* the nodal values of the computed line p = 100 cm. Then we used the **Interpolate** routine of *Mathematica* to make the function $z_{100}(x)$. After that we integrated by the **NIntergate** routine of *Mathematica*:

$$S_{100} = -2\int_0^{200} z_{100}(x)\mathrm{d}x\,. \tag{5}$$

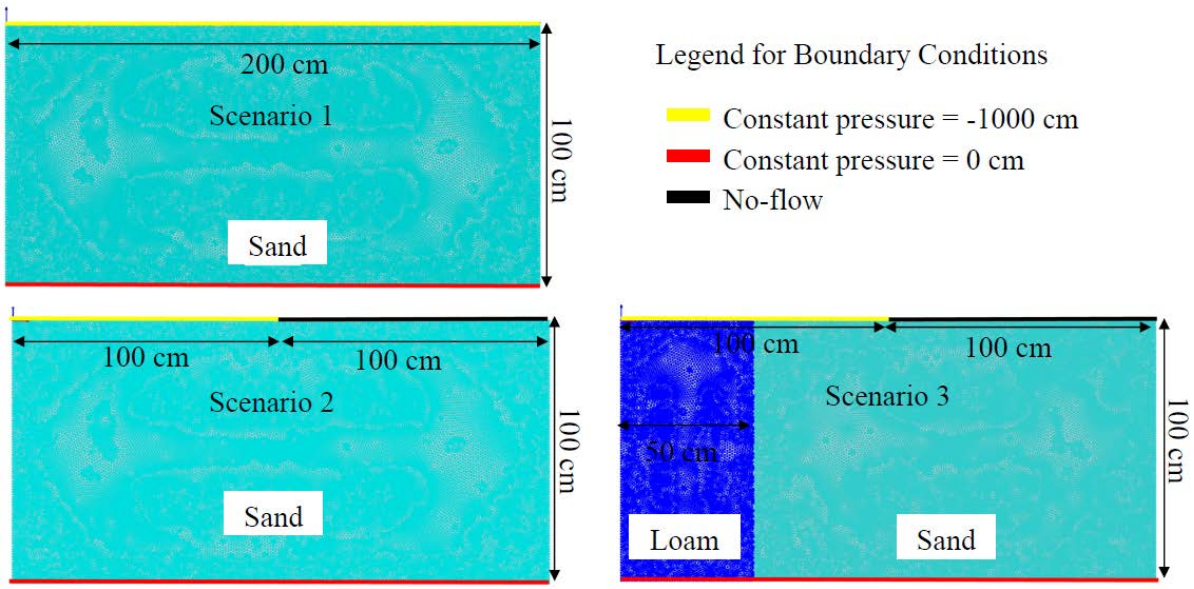

Fig.10. Domain discretization and HYDRUS boundary conditions for the three scenarios (no pavement and no wick, pavement without wick, and pavement with wick) and an effective homogenous rectangular flow domain.

The isobars at the final time of simulations i.e. t = 10 years for all scenarios are shown in Fig. 11. Computations of Z_M(cm) and S_{100} (cm^2) for the five-layered soil profile and the three scenarios are presented in Table 3. In scenario 1, Z_M = -11.8 cm and S_{100} = 4720 cm^2. However, the no-flow horizontal segment in scenario 2, have remarkably increased Z_M and decreased S_{100}. A wick of loamy sand in scenario 3 dramatically increased S_{100} by 1.1 and 1.9 times as compared with scenarios 1 and 2, respectively. This proves that mosaic porous domains with engineered capillary siphons can function as intelligently designed substrates (see similar controls of moisture and solute fluxes in topsoils, Al-Maktoumi et al., 2014, Al-Mayahi et al., 2020, Al-Mazroui et al., 2020).

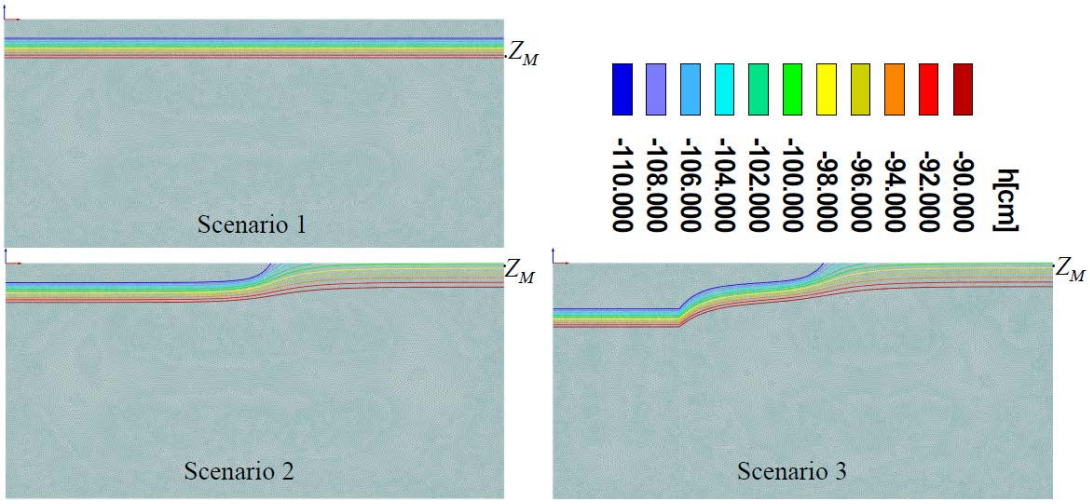

474

475 **Fig.11.** HYDRUS isobars at t = 3650 days for three scenarios in Fig.10.

476 **Table 3:** HYDRUS-computed criteria of waterlogging.

Criteria of waterlogging	Five layered soil profile	Scenario 1	Scenario 2	Scenario 3
Z_M(cm)	-35.44	-11.8	-0.10	-0.03
$S100$ (cm^2)	14176	4720	2617.37	5060.42
Q (cm^2/day)	361574.62	0.0024	0.0018	1.58

477

478 It is noteworthy that numerous data sets of geometrical-hydraulic parameters of the wick were
479 tested before we encountered such a beautiful dewatering effect presented in Fig.11. In our
480 searches, we did not have any algorithm (to be developed in the future) but followed what is
481 similar to "wild cat" drilling.

482 ## 6. Concluding Remarks on Perspectives

483 Our analytical solutions, 2-D MODFLOW and HYDRUS simulations show that a
484 shallow pristine water table with direct evaporation to the vadose zone-atmosphere can
485 significantly rise if a part of the soil surface becomes impermeable (pavement or other urban
486 development which impedes or blocks evaporation). In the simplest scenario of seawater
487 seepage into a coastal aquifer from a vertical shoreline with an impermeable downstream vertical
488 boundary, and for 1-D steady-state Dupuit-Forcheheimer model, revealed a counterintuitive

result: the area of the vadose zone above the water table, which can be considered as a criterion of waterlogging, varied non monotonically with variations of the locus of the evaporation-blocking segment on the ground surface, provided that the width of the segment is fixed.

A standard method to combat waterlogging in urban shallow aquifers is horizontal or vertical drainage with the pumping of the drained water. We suggest an alternative, energy-passive and zero-CO_2 emission technique: a wick-wall which barriers the incident unconfined groundwater flow, intercepts part of it and evaporates to the atmosphere. Such a capillary siphon can envelope a building and home garden as illustrated in Fig.1b. Our MODFLOW and HYDRUS 2-D simulations illustrate the potentiality of controlling water logging and even amplifying evaporation in urban areas with shallow water table rise. Further modeling of 3-D saturated-unsaturated flows in the vicinity of real buildings in the study area (coastal zone, Muscat, Oman) is needed for assessments of the water table drawdown and soil's desaturation near buildings' footings and in the root zone of cultivated plants. Also, an economic analysis of such wick-wall technology is necessary.

We believe that an intelligent design of land cover (optimal sizes and loci of impermeable barriers, like one in Fig.1, on the ground surface) and controlling of the structure of porous media (i.e. making porous composites) groundwater inundation can be mitigated. Moreover, recently we put forward the concept of MAD (Managed Aquifer Discharge) by optimization of exfiltrating engineering structures (trenches, pits, slack water ponds), which drain (exfiltrate) the nearby waterlogged soils (Kacimov et al., 2020), in full symmetry to standard MAR projects which aim at infiltrating water into the subsurface (Maliva, 2020). The perspectives of future studies stemming from our work are fascinating, both in further modeling and engineering implementations.

In this paper, we studied capillary siphons modeled as fine-textured rectangles, which fully penetrate the aquifer from the soil surface to the bedrock (Section 4 and Appendix) or

514 shallow water table (Section 5). Both the shape and size of these entities shown in Fig.1b,c,
515 which verticalize and evaporates a quasi-horizontal groundwater flow, can be varied (see e.g.
516 experiments in Papafotiou et al. 2010).

517 We simulated siphons as homogeneous fine-textured lenses. Optimal layering (graded
518 siphons) can be explored in 2-D saturated-unsaturated flows, similar to Kacimov et al. (2019b) in
519 1-D flows. Siphons's shapes, more complex than rectangles assumed in this paper, can be
520 considered. HYDRUS3D can be used for modeling rectangular parallelepipeds and 3-D barriers
521 (see e.g. Al-Mayahi et al., 2020) rather than rectangles as flow domains and strips as 2-D barriers
522 in this paper.

523 The impervious pavement in Fig.1a was modeled as a solitary impermeable segment of
524 width *d*. Multiple no-flow segments can be easily examined in the analytical DF 1-D theory and
525 numerically. Buried foundations occluding groundwater motion (like ones in De Caro et al. 2020
526 and Medovar et al. 2018) can be modeled both analytically by the potential 2-D theory (Ilyinsky
527 and Kacimov 1991) and numerically by MODFLOW and HYDRUS.

528

529 **Appendix. Analytical Solution for Tension-Saturated Flow in Wick**

530 In this Appendix, we consider a simplified geometry of a rectangular wick *ABCD* (Fig.
531 A.1) with the water table dipping towards it from a vertical constant piezometric head boundary,
532 similarly to Section 3. Unlike the DF capillarity-free model of Section 3, here we use the
533 Vedernikov-Bouwer potential model (Kacimov et al., 2019a) of a saturated-tension saturated
534 flow in a vertical cross-section.

535 We introduce a system of Cartesian coordinates O*xy*, the abscissa axis of which is counter
536 oriented with Ox_c. The wick in Fig.1a is a rectangular domain G_z. Along a vertical segment *AD*
537 of a size h_D the siphon receives saturated water from the aquifer. First, we assume that h_D is a
538 given constant (obtained, say, from simulations in Section 3). We assume that along the line *AD*

the hydraulic head is constant i.e. for seepage inside G_z the aquifer on the right of the siphon acts like a surface-water reservoir. This assumption is suitable if $K_{s1}<<K_s$ and is similar to one in the problem of the conjugation of seepage in clay cores of earth dams and their coarse shoulders (Kacimov et al., 2020a).

We assume that seepage in G_z is Darcian, steady-state, and tension saturated above the phreatic line DF. We introduce a complex physical coordinate $z=x+iy$. The total hydraulic head, $h(x,y)$ in G_z and the Darcian velocity, $\vec{V}(x,y)$ are related as:

$$\vec{V} = -K_{s1}\nabla h. \quad \text{(A1)}$$

The complex potential is $w(x,y)=\varphi+\mathrm{i}\psi$, where $\varphi=-K_{s1}h$ is the velocity potential, and ψ is the stream function. In the Vedernikov-Bouwer (VB) model, φ and ψ, as well as the pressure head $p(x,y)=-\varphi/K_{s1}-y+c_p$, obey the Laplace equation. We select D in Fig..1a as a fiducial point where we set w=0 and, therefore, $\varphi_{AD}=0$ and $c_p=h_D$.

The segments DB and OC in G_z are impermeable, the former due to a capillary barrier between the fine wick and coarse aquifer and the latter as a lateral confining of our flow domain from the left in Fig.1a. Therefore, $\psi_{DB}=0$, $\psi_{AOC}=Q$ where the seepage flow rate, Q, through G_z is a part of the solution. Along BC the pressure head $p=-p_{BC}$, $0<p_{BC}<p_C$ where p_C is a given positive constant for a given soil, a parameter of the VB model, which quantifies the capillary properties of the wick. PK-77 reports p_C from tens of cm for sandy soils up to tens of meters for clays. The value of p_{BC} depends on atmospheric conditions (see a similar isobaricity condition, which we imposed in Section 4 along the soil surface in HYDRUS simulations). Then along BC the velocity potential $\varphi=\varphi_B=K_{s1}(p_{BC}+h_D-r)$. For water to be wicked to the atmosphere the inequality should hold $\varphi_B>0$. A dashed line FD in Fig.1a is a phreatic curve p = 0 in G_z. Thus, in the complex potential domain, we have a rectangle G_w (Fig.A1).

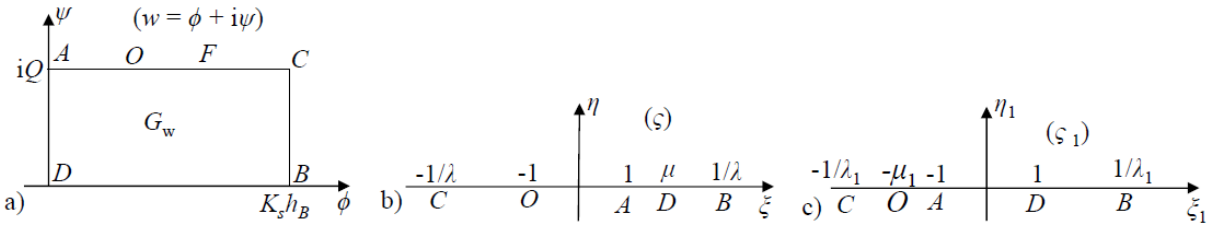

Fig.A1. a) Complex potential domain in the VB model; b) reference plain ς ; c) reference plain ς_1.

We map conformally G_w onto G_z using two reference planes $\varsigma = \xi + \mathrm{i}\eta$ and $\varsigma_1 = \xi_1 + \mathrm{i}\eta_1$ shown in Fig.A1b and Fig.A1c, correspondingly. By the Schwarz-Christoffel integral

$$z(\varsigma) = \frac{b}{2} + \frac{b}{2K(\lambda)} \int_0^{\varsigma} \frac{\mathrm{d}t}{\sqrt{(1-t^2)(1-\lambda^2 t^2)}} = \frac{b}{2} + \frac{b}{2K(\lambda)} F(\arcsin\varsigma, \lambda). \qquad \text{(A2)}$$

The upper half-plane $\varsigma > 0$ is mapped onto the domain G_z with the correspondence of points $C \to -1/\lambda$, $O \to -1, A \to 1, B \to 1/\lambda$ $(0 < \lambda < 1)$. Here $F(\arcsin\varsigma, \lambda)$ and $K(\lambda)$ are incomplete and complete elliptic integrals of the first kind (see Abramowitz and Stegun, 1969, formulae 17.2.7, 17.3.1). From eqn.(A2), we have $z(1/\lambda) = b + \mathrm{i}r$ and $F(\arcsin 1/\lambda, \lambda) = K(\lambda) + \mathrm{i}\,K'(\lambda)$ that gives

$$K'(\lambda) / K(\lambda) = 2r / b, \qquad \text{(A3)}$$

where $K'(\lambda) = K(\lambda')$, $\lambda' = \sqrt{1-\lambda^2}$. In eqn.(A.3) we use the **FindRoot** routine of *Mathematica* and determine the modulus λ of the elliptic integrals. An accurate asymptotic representation for λ is

$$\lambda \cong 4\exp(-\pi r / b) \quad \text{if} \quad r >> b \,.$$

The image of point *D* in the half-plane of Fig.A2b is $\varsigma = \mu$. The positive parameter μ ($\varsigma < \mu < 1/\lambda$) satisfies the condition $z(\mu) = b + \mathrm{i}h_D$. From eqn.(A.3) and formula (1.2.64.1) from Prudnikov et al. (2002) we get:

$$h_D = \frac{b}{2K(\lambda)} \int_1^{\mu} \frac{\mathrm{d}\tau}{\sqrt{(\tau^2-1)(1-\lambda^2\tau^2)}} = \frac{r}{K'(\lambda)} F\left(\arcsin\left(\frac{\sqrt{\mu^2-1}}{\lambda'\mu} \right), \lambda' \right). \qquad \text{(A4)}$$

The relation (A.4) is an equation with respect to μ, if parameters *b*, *r*, h_D are fixed, and the corresponding modulus λ is determined from (A.3). The approximate formula

$$\mu = 0.5 \exp\left[h_D K'(\lambda) \right], \qquad \text{(A5)}$$

which solves eqn.(A4), was used in our computations below.

The second reference plane is needed for mapping of the complex potential rectangle, *viz*. we map G_w onto the upper half-plane $\varsigma_1 > 0$, with the correspondence of the points $C \to -1/\lambda_1$, $A \to -1$, $D \to 1$, $B \to 1/\lambda_1$, where $0 < \lambda_1 < 1$. The corresponding Schwarz-Christoffel integral is:

$$w(\varsigma_1) = \frac{\mathrm{i}Q}{2} - \frac{\mathrm{i}Q}{2K(\lambda_1)} \int_0^{\varsigma_1} \frac{\mathrm{d}t}{\sqrt{(1-t^2)(1-\lambda_1^2 t^2)}} = \frac{\mathrm{i}Q}{2} - \frac{\mathrm{i}Q}{2K(\lambda_1)} F(\arcsin \varsigma_1, \lambda_1). \qquad \text{(A6)}$$

As $w(1/\lambda_1) = K_{s1} h_b$ (see Fig.A1a), then from eqn.(A.6) and the equality $F(\arcsin(1/\lambda_1), \lambda_1) = K(\lambda_1) + \mathrm{i}K'(\lambda_1)$ follows:

$$\frac{2K}{K'} = \frac{Q}{K_{s1} h_b}, \qquad \text{(A7)}$$

where $K = K(\lambda_1)$, $K' = K(\lambda_1')$, and $\lambda_1' = \sqrt{1-\lambda_1^2}$.

Next, the ς-half-plane (Fig.A1b) is mapped onto the ς_1-half-plane (Fig.A1c). This is done by the Mobius transformation which is uniquely defined by fixing the relation of three pairs of points: $-1/\lambda \to -1/\lambda_1, 1 \to -1, 1/\lambda \to 1/\lambda_1$. Then the mapping function is determined from the following relation :

$$\frac{\varsigma + 1/\lambda}{\varsigma - 1}(1-\lambda) = \frac{\varsigma_1 + 1/\lambda_1}{\varsigma_1 + 1}(1+\lambda_1). \qquad \text{(A8)}$$

Due to the correspondence of points *O* and *D* in the two reference half-planes, we put $\varsigma = 1$ and $\varsigma = \mu$ into the left-hand side of eqn.(A8), $\varsigma_1 = -\mu_1$ and $\varsigma_1 = 1$ into the right-hand side of this equation and obtain

$$\frac{(1-\lambda)^2}{2\lambda} = \frac{\mu_1 - 1/\lambda_1}{\mu_1 - 1}(1+\lambda_1), \qquad \frac{\mu + 1/\lambda}{\mu - 1}(1-\lambda) = \frac{(1+\lambda_1)^2}{2\lambda_1}\,. \tag{A9}$$

The second eqn.(A9) is a quadratic equation with respect to λ_1 (we remind that parameters λ and μ are determined earlier by eqns. (A.3) and (A.5) respectively). The root of this equation, satisfying the condition $0 < \lambda_1 < 1$, is given by the formula:

$$\lambda_1 = s - \sqrt{s^2 - 1}, \qquad s = \frac{1/\lambda - \mu\lambda}{\mu - 1} > 1\,. \tag{A10}$$

We introduce dimensionless quantities: ($h_D^*, b^*, d^*, h_B^*, V^*, Q^*$)=($h_D/r$, b/r, p_B/r, V/K_{s1}, $Q/(K_{s1}\,r)$) and drop the asterisks for dimensionless quantities. In Fig.A2 we plot the graphs of the functions $Q(b)$ at $h_B = 0.3$ and $h_D = 0.3, 0.5, 0.7$ (curves 1-3) .

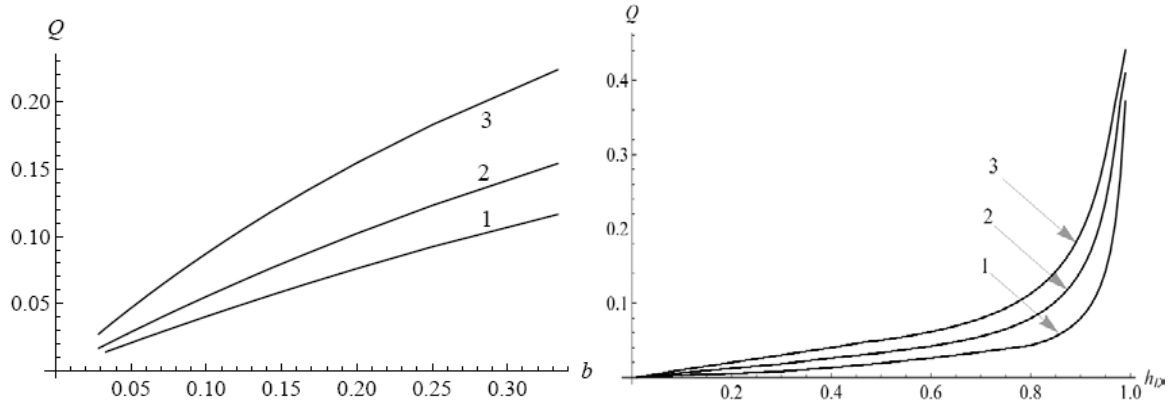

Fig.A2. Seepage flow rate through the wick: as function of its width at $h_B = 0.3$ and $h_D = 0.3, 0.5, 0.7$(curves 1-3), left panel; as function of the size of the "hydraulic window", through which groundwater infiltrates, at $h_B = 0.3$ and $b = 0.03, 0.06, 0.09$ (curves 1-3), right panel.

Fig.A2, left panel shows the graphs $Q(b)$ for $h_B = 0.3$ and $h_D = 0.3, 0.5, 0.7$ (curves 1-3). Obviously, in the limit $b \to 0$ the flow rate approaches zero i.e. all three curves collapse to the origin of coordinates. However, in this limit of "thin" siphons, Mathematica stumbles with computation of elliptic integrals. Fig.A2, right panel shows the graphs $Q(h_D)$ for $h_B = 0.3$ and *b*

620 = 0.03, 0.06, 0.09 (curves 1-3) . These graphs that illustrate for the selected h_D and b if h_D is high
621 enough (greater than about 0.7), then the flow rate increases highly nonlinearly and rapidly with
622 h_D.

623 **Acknowledgments**

624 This work was supported by SQU, grants "Rise of Water-table and its Mitigation at SQU
625 Campus - IG/VC/WRC/21/01" and it was carried out as part of the development program of the
626 Scientific and Educational Mathematical Center of the Volga Federal District, agreement No.
627 075-02-2020-1478.. Dr. I.R.Kayumov kindly helped with the derivation of eqn. (A5). This work
628 is part of the research activities of a registered research group at SQU: DR/RG/17. Helpful
629 comments rendered by a Referee are appreciated.

630

631 **References**

632 +Abramowitz, M., Stegun, I.A.:Handbook of Mathematical Functions. Dover, New York.,
633 (1969).

634 +Abu-Rizaiza, O.S.: Threats from groundwater table rise in urban areas in developing countries.
635 Water International, 24(1), 46-52. (1999).

636 + Abu-Rizaiza, O.S., Sarikaya, H.Z., Khan, M.A.: Urban groundwater rise control: case study. J.
637 of Irrigation and Drainage Engineering ASCE, 115(4), 588-607 (1989)

638 + Aliewi, A., Al-Qallaf, H., Rashid, T., Al-Odwani, A.: Hydraulic evaluation of a dewatering
639 scheme in shallow aquifers in Kuwait. Quarterly Journal of Engineering Geology and
640 Hydrogeology, 53(1), 125-136 (2020).

641 +Al-Hamami, S. Rising groundwater level in Muscat airport and its impacts. B.Sc. Thesis,
642 Department of Earth sciences, Sultan Qaboos University, Oman (2019).

643 + Al-Maktoumi, A., Al-Ismaily, S., Kacimov, A., Al-Busaidi, H., Al-Saqri, S., Al-Haddabi, M.:
644 Soil substrate as a cascade of capillary barriers for conserving water in a desert environment:
645 lessons learned from arid nature. J. Arid Land, 6(6), 690-703 (2014)

646 +Al-Mayahi, A. Al-Ismaily, S., Al-Maktoumi, A., Al-Busaidi, H., Kacimov, A., Janke, R.,
647 Bouma, J., Šimůnek J.:A smart capillary barrier-wick irrigation system: A new technique for
648 water conservation for home gardens in arid zones. Irrigation Science, 38(3), 235-250 (2020)

649 +Al-Mazroui, M., Al-Yahyai, R., Al-Ismaily, S., Kacimov, A.: Evaluation of potting media for
650 marigold under salinity stress condition. J. of Applied Horticulture, 22(1), 49-56 (2020).

+Al-Sefry, S.A., Şen, Z:. Groundwater rise problem and risk evaluation in major cities of arid lands–Jedddah case in Kingdom of Saudi Arabia. Water Resources Management, 20(1), 91-108 (2006)

+Al-Senafy, M.: Management of water table rise at Burgan oil field, Kuwait. Emirates J. for Engineering Research, 16 (2), 27-38 (2011).

+Al-Senafy, M., Hadi, K., Fadlelmawla, A., Al-Fahad, K., Al-Khalid, A., Bhandary, H.: Causes of groundwater rise at Al-Qurain residential area, Kuwait. Procedia Environmental Sciences, 25, 4-10 (2015).

+Al-Shukaili, A. Al-Busaidi, H., Al-Maktoumi, A., Abdalla, O., Shelukhina, O., and Kacimov, A.R. Oblique porous composite as evaporating "cap": Do desert dunes preserve moisture by capillary barriers and tilt of their slopes? *Water Resources Research* ,55, 2504–2520 (2019).

+Al-Washahi, A., 2019. The causes of rising groundwater level in Al-Amerat Area. B.Sc. Thesis, Department of Earth sciences, Sultan Qaboos University, Oman (2019).

+Attard, G., Winiarski, T., Rossier, Y., Eisenlohr, L.: Impact of underground structures on the flow of urban groundwater. Hydrogeology J., 24(1), 5-19 (2016).

+ Awad, S. R., and El Fakharany, Z. M. : Mitigation of waterlogging problem in El-Salhiya area, Egypt. Water Science, 34(1), 1-12 (2020).

+Barron, O. V., Donn, M. J., Barr, A. D.:Urbanisation and shallow groundwater: Predicting changes in catchment hydrological responses. Water Resources Management, 27, 95–115 (2013).

+Bob, M., Rahman, N., Elamin, A., Taher, S.: Rising groundwater levels problem in urban areas: a case study from the Central Area of Madinah City, Saudi Arabia. Arabian Journal for Science and Engineering, 41(4), 1461-1472 (2016).

+Boettinger, J.L.: Aquisalids (Salorthids) and other wet saline and alkaline soils: problems identifying Aquic conditions and Hydric soils 1. Aquic conditions and hydric soils: The problem soils, (aquicconditions), 79-97 (1997).

+Boettinger, J.L, Richardson, J.L.: Saline and wet soils of wetlands in dry climates. Wetland Soils: Genesis, Hydrology, Landscapes, and Classification., 383-390 (2001).

+Brostoff, W. N., Sharifi, M.R., Rundel, P.W.: Primary productivity of cryptobiotic crusts of a seasonally inundated system of pans and dunes at Edwards Air Force Base, Western Mojave Desert, California: Laboratory studies. Flora, 197, 143–151 (2002).

+Capelli, G., Mazza, R., and Papiccio, C.: Intrusione salina nel Delta del Fiume Tevere. Geologia, idrologia e idrogeologia del settore romano della piana costiera. Giornale di Geologia Applicata, 5, 13-28 (in Italian) (2007).

+Cardarelli, E., De Donno, G., Scatigno, C., . Oliveti, I., Preite Martinez, M., Prieto-Taboada, N. Geophysical and geochemical techniques to assess the origin of rising damp of a Roman building (Ostia Antica archaeological site). Microchemical J., 129, 49-57 (2016).

+Chaudhary, M.T.A.: Implications of rising groundwater level on structural integrity of underground structures – investigations and retrofit of a large building complex. Structural Survey, 30(2), 111-129 (2012).

+Coffey, T. S., and Shaw, J. B.: Congruent bifurcation angles in river delta and tributary channel networks. Geophysical Research Letters, 44(22), 11,427-11,436 (2017).

+Cohen, Y., and Rothman, D.H.: .Exact solution for the Poisson field in a semi-infinite strip. Proceedings of the Royal Society A: Mathematical, Physical and Engineering Sciences 473, 20160908 (2017).

+Cramer, V. A., Hobbs, R. J.: Ecological consequences of altered hydrological regimes in fragmented ecosystems in southern Australia: impacts and possible management responses. Austral Ecology, 27(5), 546-564 (2002).

+ Craster, R.V.: Two related free boundary problems. IMA Journal of Applied Mathematics, 52(3), 253-270 (1994).

+ De Caro, M., Crosta, G. B., Previati, A.: Modelling the interference of underground structures with groundwater flow and remedial solutions in Milan. Engineering Geology, 105652 (2020).

+Essam, D., Ahmed, M., Abouelmagd, A., and Soliman, F. Monitoring temporal variations in groundwater levels in urban areas using ground penetrating radar. Science of The Total Environment, 703, 134986 (2020).

+Haitjema, H. M.: Analytic Element Modeling of Groundwater Flow. Elsevier (1995).

+Howard, K.W., Israfilov, R.G. eds.: Current Problems of Hydrogeology in Urban Areas, Urban Agglomerates and Industrial Centres (NATO Science Series, Vol. 8). Springer, Dordrecht (2012).

+Ilyinsky, N.B., Kacimov, A.R.: Estimates of backwater and drying levels in hydrodynamic model. Fluid Dynamics, 26(2), 224-231 (1991).

+Jha, A.K., Bloch, R., Lamond, J.: Cities and Flooding: a Guide to Integrated Urban Flood Risk Management for the 21st Century. The World Bank, Washington, DC (2012).

+Kacimov, A.R., Obnosov, Yu.V.: Analytic solution to a problem of seepage in a checker- board massif. Transport in Porous Media, 28 (1), 109-124 (1997).

+Kacimov, A.R., Sherif, M.M., Perret, J.S., Al-Mushikhi, A.: Control of sea-water intrusion by salt-water pumping: Coast of Oman. Hydrogeology J., 17, 541-558 (2009).

+Kacimov A.R., Abdalla O.: Water table response to a tidal agitation in a coastal aquifer: The Meyer–Polubarinova-Kochina theory revisited. J. Hydrology, 392. 96–104 (2010). doi:10.1016/j.jhydrol.2010.07.040

+ Kacimov A., Al-Maktoumi, A. and Šimůnek J.: Water table rise in urban shallow aquifer with vertically-heterogeneous soils: Girinskii's potential revisited. Hydrological Sciences J. (in press) (2021a) https://doi.org/10.1080/02626667.2021.1890327 .

+Kacimov, A., Obnosov ,Yu.V., Or, D.: Evaporation induced capillary siphoning through hydraulically connected porous domains: the Vedernikov-Bouwer model revisited. Transport in Porous Media,129, p.231–251 (2019a),https://doi.org/10.1007/s11242-019-01285-z.

+Kacimov, A., Obnosov, Yu.V., Simunek, J.: Minimal evaporation by optimal layering of topsoil: Revisitng Ovsinsky's smart mulching-tillage technology via Gardner-Warrick's unsaturated analytical model and HYDRUS. Water Resources Research,55(5), 3606-3618 (2019b).

+Kacimov, A., Obnosov Yu.V. and Simunek, J.: Seepage to ditches and topographic depressions in saturated and unsaturated soils. Advances in Water Resources, 103732 (2020b).

+Kacimov, A., Yakimov, N.D., Simunek, J.: Phreatic seepage flow through an earth dam with an impeding strip. Computational Geosciences. 24, 17–35 (2020a).

+Kazemi, G.L.: Impacts of urbanization on the groundwater resources in Shahrood, Northeastern Iran: Comparison with other Iranian and Asian cities. Physics and Chemistry of the Earth, 36, 150–159 (2011).

+Knott, J. F., Elshaer, M., Daniel, J. S., Jacobs, J. M., Kirshen, P.: Assessing the effects of rising groundwater from sea level rise on the service life of pavements in coastal road infrastructure. Transportation Research Record, *2639*(1), 1-10 (2017).

+Kreibich, H., Thieken, A.H.: Assessment of damage caused by high groundwater inundation. Water Resources Research, 44, W09409 (2008).

+Kreibich, H., Thieken, A. H., Grunenberg, H., Ullrich, K., Sommer, T.: Extent, perception and mitigation of damage due to high groundwater levels in the city of Dresden, Germany. Natural Hazards and Earth System Sciences (NHESS), 9(4), 1247-1258 (2009).

+Lerner, D. N. ed.: Urban Groundwater Pollution: IAH International Contributions to Hydrogeology 24. Balkema, Lisse (2003).

+Lerner, D. N., Harris, B.:The relationship between land use and groundwater. resources and quality. Land Use Policy, 26S, S265–S273 (2009).

+Lichvar, R., Brostoff, W.,Sprecher, S.: Surficial features associated with ponded water on playas of the arid southwestern United States: indicators for delineating regulated areas under the Clean Water Act. Wetlands, 26(2),385-399 (2006).

+ Maliva, R. G.: Anthropogenic Aquifer Recharge. Springer, Cham (2020).

+Mancini, C.P., Lollai, S., Volpi, E. and Fiori, A.: Flood Modeling and Groundwater Flooding in Urbanized Reclamation Areas: The Case of Rome (Italy). Water, 12(7), p.2030 (2020).

+McGrane, S.J.: Impacts of urbanization on hydrological and water quality dynamics, and urban water management: a review. Hydrological Sciences J., 61(13), 2295-2311 (2016).

+Medovar, Y.A., Yushmanov, I.O., Bronskaya, E.E.:Changes in the ecological condition of a territory at the construction of buildings with a deep foundation under various geological conditions in Moscow.Water Resources, 45(2), 65-72 (2018).

+Minnig, M., Moeck, C., Radny, D.,Schirmer, M.: Impact of urbanization on groundwater recharge rates in Dübendorf, Switzerland. J. of Hydrology, 563, 1135–1146 (2018).

+Mubarek, E. E. Causes of rising groundwater level in Al Ansab area: chemical, biological and isotopic approaches. M.Sc. Thesis, Department of Biology, Sultan Qaboos University, Oman (2018).

+Naik, P.K., Tambe, J.A., Dehury, B.N., Tiwari, A.N.: Impact of urbanization on the groundwater regime in a fast growing city in central India. Environmental Monitoring and Assessment, 146(1-3), 339-373 (2008).

+Papafotiou, A., Schütz, C., Lehmann, P., Vontobel, P., Or, D., Neuweiler, I.: Measurement of preferential flow during infiltration and evaporation in porous media. Bulletin of the Geological Society of Greece, 43 (4), 1831-1839 (2010).

+Polubarinova-Kochina, P.Ya.: Theory of Ground Water Movement. Nauka, Moscow (in Russian) (1977).

+Porse, E., Glickfeld, M., Mertan, K., Pincetl, S.: Pumping for the masses: evolution of groundwater management in metropolitan Los Angeles. GeoJournal, 81(5), 793-809 (2016).

+Preene, M., Fisher, S.: Impacts from groundwater control in urban areas. Proceedings of the XVI ECSMGE, 2847-2852 (2015).

+Prudnikov, A.P., Brychkov, Yu. A., Marichev, O.I.: Integrals and Series. Elementary Functions, Vol. 1, Gordon & Breach Science Publishers, New York.; Translated from the Russian and with a preface by N. M. Queen (1986).

+Saunders, D. A.: Ecological consequences of clearing and fragmentation of native vegetation. In Proceedings of the National Malleefowl Forum (pp. 96-99) (2004).

+Schirmer, M., Leschik, S., Musolff, A.: Current research in urban hydrogeology–A review. Advances in Water Resources, 51, 280-291 (2013).

+ Simcore Software: Processing Modflow: An Integrated Modeling Environment for the Simulation of Groundwater Flow, Transport and Reactive Processes (2012).

+Šimůnek, J., Van Genuchten, M.T., Šejna, M.: Recent developments and applications of the HYDRUScomputer software packages. Vadose Zone J., 15(7) (2016).

+Soil Science Division Staff.: Soil Survey Manual. In: USDA Handbook 18 (eds C. Ditzler, K. Scheffe & H.C. Monger). Government Printing Office, Washington, DC (2017).

+Strack, O.D.L.: Groundwater Mechanics. Prentice Hall, Englewood Cliffs (1989).

+Vázquez-Suñé, E., Sánchez-Vila, X., Carrera, J.: Introductory review of specific factors influencing urban groundwater, an emerging branch of hydrogeology, with reference to Barcelona, Spain. Hydrogeology J., 13(3), 522-533 (2005).

+Vogwill, R. ed.: Solving the Groundwater Challenges of the 21st Century (Vol. 22). CRC Press, Boca Raton (2016).

+Wolfram, S.: *Mathematica.* A System for DoingMathematics by Computer. Addison-Wesley, Redwood City (1991).

+Wood, W., Rizk, Z.S., Alsharhan, A.S.: Timing of recharge, and the origin, evolution and distribution of solutes In:“Water Resources Perspectives: Evaluation, Management and Policy”, Edited by Wood, W. W. and Alsharhan, A. S., Elsevier, 295-312 (2003).

+Yeh, T.C., Khaleel, R., Carroll, K.C.: Flow Through Heterogeneous Geologic Media. Cambridge University Press (2015).

+Yechieli, Y., Wood, W. W. Hydrogeologic processes in saline systems: playas, sabkhas, and saline lakes. Earth-Science Reviews, 58(3-4), 343-365 (2002).

811

812 **Figure Captions**

813 Fig. 1. a) Vertical cross-section of an unconfined coastal aquifer. Seawater seeps through a
814 vertical coastal segment E_3M_3 and moves over an impermeable horizon inland, driven by
815 evaporation from the ground surface CBM_3. The left-most boundary, a vertical segment *ADB*,
816 An strip impervious to evaporation of the land surface has a width d and located distance u_1
817 from the shoreline. A fully-penetrating wick-wall *OCBA* of a width b is made of fine-textured
818 soil (impeding and facilitating evaporation). The wick-wall may be located on the left of a
819 vertical segment *ADB*, distance a from the shoreline. If no wick, then *ADB* is impermeable; b)
820 aerial view of a rectangular area protected by a wick-wall; c) groundwater flow topology in the
821 vicinity of a partially-penetrating wick-wall (vertical cross-section).

822 Fig. 2. Virgin and evaporation-eliminated water tables $h(x_c)$and $h_v(x_c)$for $h_0 = 0.15$, $e = 0.01$,
823 $u_1 = 0.5$, $d = 0.2$ (curves 1 and 2, respectively). Curves 3 and 4 are plotted for $h_0 = 0.1$, $e = 0.01$,
824 $u_1 = 0.3$, $d = 0.2$.

825 Fig.3. "Dry area" S_d as a function of u_1 for three strip width $d = 0.1$, 0.5 and 0.7 (curves 1-3)
826 at $h_0 = 0.1$ and $e = 0.001$.

827 Fig.4. a) Maximal (optimal) "dry area" S_{dm} as a function of h_0 for $e_0 = 0.01$.

828 b) Optimal $u_{1m}(h_0)$ and $d_m(h_0)$ (curves 1, 2, correspondingly) for $e_0 = 0.01$.

829 Fig. 5. A vertical cross-section of a rectangular flow domain for the problem simulated by
830 MODFLOW.

831 Fig.6. MODFLOW-computed equipotential lines without capillary with and with wick
832 (upper and lower panels).

833 Fig.7.MODFLOW streamlines for flow without a wick (upper panel), with wick (middle
834 panel) and refraction in a zoomed zone close to the interface between two subdomains of
835 contrasting conductivity (lower panel).

836 Fig.8. Water tables for a homogeneous and composite aquifers.

837 Fig.9. HYDRUS isobars at $t = 3650$ days for a pristine five-layered soil profile from the Al-
838 Mawaleh site.

839 Fig.10. Domain discretization and HYDRUS boundary conditions for the three scenarios (no
840 pavement and no wick, pavement without wick, and pavement with wick) and an effective
841 homogenous rectangular flow domain.

842 Fig.11. HYDRUS isobars at $t = 3650$ days for three scenarios in Fig.10.

843 Fig.A1. a) Complex potential domain in the VB model; b) reference plain ς ; c) reference
844 plain ς_1 .

845 Fig.A2. Seepage flow rate through the wick: as function of its width at $h_B = 0.3$ and $h_D = 0.3$,
846 0.5, 0.7(curves 1-3), left panel; as function of the size of the "hydraulic window", through which
847 groundwater infiltrates, at $h_B = 0.3$ and $b = 0.03$, 0.06, 0.09 (curves 1-3), right panel.

List of Acronyms

MSL	Mean Sea Level
ODE	Ordinary Differential Equation
BVP	Boundary Value Problem
PK-77	Polubarinova-Kochina, P.Ya., 1977. Theory of Ground Water Movement. Nauka, Moscow (in Russian)
VB	Vedernikov-Bouwer